Available online at www.sciencedirect.com

ScienceDirect

Geochimica et Cosmochimica Acta 183 (2016) 250–266

Geochimica et Cosmochimica Acta

www.elsevier.com/locate/gca

The transfer of seasonal isotopic variability between precipitation and drip water at eight caves in the monsoon regions of China

Wuhui Duan [a,*], Jiaoyang Ruan [b,c], Weijun Luo [d], Tingyong Li [e], Lijun Tian [a], Guangneng Zeng [d], Dezhong Zhang [f], Yijun Bai [g], Jilong Li [h], Tao Tao [a,i], Pingzhong Zhang [g], Andy Baker [j], Ming Tan [a,*]

[a] *Key Laboratory of Cenozoic Geology and Environment, Institute of Geology and Geophysics, Chinese Academy of Sciences, China*
[b] *State Key Laboratory of Biogeology and Environmental Geology, China University of Geosciences, Wuhan, China*
[c] *Laboratoire des Sciences du Climat et de l' Environnement, Gif-sur-Yvette, France*
[d] *State Key Laboratory of Environmental Geochemistry, Institute of Geochemistry, Chinese Academy of Sciences, China*
[e] *School of Geographical Sciences, Southwest University, China*
[f] *College of Earth and Environmental Sciences, Lanzhou University, China*
[g] *Key Laboratory of Mineral Resources in Western China (Gansu Province) and School of Earth Sciences, Lanzhou University, China*
[h] *Key Laboratory of Virtual Geographic Environment, Ministry of Education, Nanjing Normal University, China*
[i] *Institute of Geomechanics, Chinese Academy of Geological Sciences, China*
[j] *Connected Waters Initiative Research Centre, University of New South Wales, Australia*

Received 10 March 2015; accepted in revised form 30 March 2016; Available online 4 April 2016

Abstract

This study presents new stable isotope data for precipitation ($\delta^{18}O_p$) and drip water ($\delta^{18}O_d$) from eight cave sites in the monsoon regions of China (MRC), with monthly to bi-monthly sampling intervals from May-2011 to April-2014, to investigate the regional-scale climate forcing on $\delta^{18}O_p$ and how the isotopic signals are transmitted to various drip sites.

The monthly $\delta^{18}O_p$ values show negative correlation with surface air temperature at all the cave sites except Shihua Cave, which is opposite to that expected from the temperature effect. In addition, although the monthly $\delta^{18}O_p$ values are negatively correlated with precipitation at all the cave sites, only three sites are significant at the 95% level. These indicate that, due to the various vapor sources, a large portion of variability in $\delta^{18}O_p$ in the MRC cannot be explained simply by either temperature or precipitation alone.

All the thirty-four drip sites are classified into three types based on the $\delta^{18}O_d$ variability. About 82% of them are static drips with little discernable variation in $\delta^{18}O_d$ through the whole study period, but the drip rates of these drips are not necessary constant. Their discharge modes are site-specific and the oxygen isotopic composition of the stalagmites growing from them may record the average of multi-year climatic signals, which are modulated by the seasonality of recharge and potential effects of evaporation, and in some cases infiltration from large rainfall events. About 12% of the thirty-four drip sites are seasonal drips, although the amplitude of $\delta^{18}O_d$ is narrower than that of $\delta^{18}O_p$, the monthly response of $\delta^{18}O_d$ to coeval precipitation is not completely damped, and some of them follow the seasonal trend of $\delta^{18}O_p$ very well. These drips may be mainly recharged by present-day precipitation, mixing with some stored water. Thus, the stalagmites growing under them may record portions of the seasonal climatic signals embedded in $\delta^{18}O_p$. About 6% of the thirty-four drip sites are

* Corresponding authors.
E-mail addresses: duanwuhui@mail.iggcas.ac.cn (W. Duan), tanming@mail.iggcas.ac.cn (M. Tan).

http://dx.doi.org/10.1016/j.gca.2016.03.037
0016-7037/© 2016 Elsevier Ltd. All rights reserved.

medium-variability drips, with constant and relatively low $\delta^{18}O_d$ values in the wet season, but with variable and relatively high $\delta^{18}O_d$ values in the dry season, reflecting flow switching in the karst or evaporation inside the cave.
© 2016 Elsevier Ltd. All rights reserved.

Keywords: Eight caves in China; Three-year cave monitoring; Stable isotopes of precipitation and drip water

1. INTRODUCTION

The oxygen isotopic composition of speleothems ($\delta^{18}O_s$) has been used to interpret variations of past climate and atmospheric circulation (e.g. Dorale et al., 1992; McDermott et al., 1999, 2001; Wang et al., 2001, 2005; Fleitmann et al., 2003; Genty et al., 2003, 2006; Yuan et al., 2004; Spötl et al., 2006; Hu et al., 2008; Zhang et al., 2008; Cheng et al., 2009; Ma et al., 2012; Moseley et al., 2014; Duan et al., 2016). Now, with the development of high resolution sampling methods and *in situ* measurements, several studies have detected seasonally variable $\delta^{18}O_s$ which were used to explore sub-annual climatic and cave environmental signals (Kolodny et al., 2003; Treble et al., 2005, 2007; Johnson et al., 2006; D. Liu et al., 2008; Orland et al., 2009, 2012, 2014). These studies are always based on the assumption that the $\delta^{18}O_s$ broadly reflects that of the local precipitation. Consequently, when the climatic significance of $\delta^{18}O_s$ is interpreted, the isotope effects (Dansgaard, 1964) that control the oxygen isotopic composition of precipitation ($\delta^{18}O_p$) are often used. $\delta^{18}O_s$ profiles from low-latitude caves are mostly used as a proxy of local rainfall amount (Neff et al., 2001; Bar-Matthews et al., 2003; Fleitmann et al., 2004; Baker et al., 2007), whereas that from mid-high latitudes, especially in Europe, usually have been interpreted as a proxy of temperature (Lauritzen, 1995; McDermott et al., 1999, 2001; Onac et al., 2002; Genty et al., 2003, 2006; Spötl et al., 2006; Moseley et al., 2014). In addition, $\delta^{18}O_s$ has also been interpreted as variations in monsoon intensity (Wang et al., 2001, 2008; Yuan et al., 2004; Cheng et al., 2009), changes in moisture sources (Cruz, 2005; Cruz et al., 2006; Maher, 2008; LeGrande and Schmidt, 2009; Clemens et al., 2010; Dayem et al., 2010) and atmosphere circulation (Tan, 2014). In this context, the climatic signals embedded in $\delta^{18}O_s$ vary regionally, and can also be controversial, especially for Chinese $\delta^{18}O_s$ records (Clemens et al., 2010; Dayem et al., 2010; Johnson, 2011; Pausata et al., 2011; Lee et al., 2012; Wang and Chen, 2012; Tan, 2014; Z. Liu et al., 2014). Thus, to correctly interpret the climatic signals of $\delta^{18}O_s$, it is critical to identify the relative importance of the factors affecting the corresponding $\delta^{18}O_p$.

During the transmission from precipitation to drip water, processes such as seasonality of recharge (Bar-Matthews et al., 1996; Jones et al., 2000; Jones and Banner, 2003; Pape et al., 2010), mixing of water parcels of different ages (Yonge et al., 1985; Ayalon et al., 1998; Williams and Fowler, 2002; McDermott, 2004; Fairchild et al., 2006; Lachniet, 2009; Joe Lambert and Aharon, 2010; Li et al., 2011; Genty et al., 2014; Baldini et al., 2015; Comas-Bru and McDermott, 2015), evaporation in the soil and epikarst zone (Bar-Matthews et al., 1996; Ayalon et al., 1998; Denniston et al., 1999; Tang and Feng, 2001; Carrasco et al., 2006; Luo and Wang, 2008; Bradley et al., 2010; Wackerbarth et al., 2010; Cuthbert et al., 2014a; Comas-Bru and McDermott, 2015) and evaporation inside the cave (Ingraham et al., 1990; Caballero et al., 1996; Carrasco et al., 2006; Oster et al., 2012; Cuthbert et al., 2014b; Zeng et al., 2015), may modify the original signal of $\delta^{18}O_p$.

In previous research, the oxygen isotopic composition of drip waters ($\delta^{18}O_d$) has been found to (1) represent the annual or more long-term weighted average value of local $\delta^{18}O_p$ (Yonge et al., 1985; Caballero et al., 1996; Williams and Fowler, 2002; McDermott, 2004; Onac et al., 2008; Li et al., 2011; Riechelmann et al., 2011; Genty et al., 2014), (2) mirror the seasonal isotopic variations of surface precipitation (Li et al., 2000; Cruz, 2005; Van Beynen and Febbroriello, 2006; Cobb et al., 2007; Fuller et al., 2008; Genty, 2008), (3) just respond to the heavy rain events in the wet season (Bar-Matthews et al., 1996; Jones et al., 2000; Jones and Banner, 2003; Pape et al., 2010), or, (4) in arid regions, record the extent of evaporative enrichment of the drip water that occurs between recharge events (Cuthbert et al., 2014a). These studies cited above mainly focus on one cave or several caves in one area. As the karst process is complicated and individual, the $\delta^{18}O_d$ within a single cave even show some differences between each other (Bar-Matthews et al., 1996; Ayalon et al., 1998; Williams and Fowler, 2002; Van Beynen and Febbroriello, 2006; Luo et al., 2014; Genty et al., 2014). This would result in stalagmites formed from those isotopically different drip waters recording divergent palaeoclimatic signals. In general, the variations of $\delta^{18}O_d$ mostly depend on the specific discharge system rather than the climatic regime. Thereby, a detailed site-specific investigation of the relationship between large-scale climate, $\delta^{18}O_p$ variability, cave hydrology, and the $\delta^{18}O_d$ variability of different types of drip sites is essential to accurately interpret $\delta^{18}O_s$ signals.

This study aims to investigate the seasonal variations of $\delta^{18}O_p$ at a regional scale in the monsoon regions of China (MRC) and how the isotopic signals are transmitted to a variety of drip sites. An approximately three-year-long (May-2011 to April-2014) on-site rainfall and drip water monitoring program has been carried out with monthly to bi-monthly sampling intervals at eight caves in the MRC. Listed from south to north, the eight caves are Xianren cave (XR) in Yunnan Province, Baojinggong Cave (BJG) in Guangdong Province, Liangfeng cave (LF) in Guizhou Province, Furong cave (FR) in Chongqing, Penglaixian cave (PLX) in Anhui Province, Heshang cave (HS) in Hubei Province, Wanxiang cave (WX) in Gansu Province and Shihua cave (SH) in Beijing (Fig. 1).

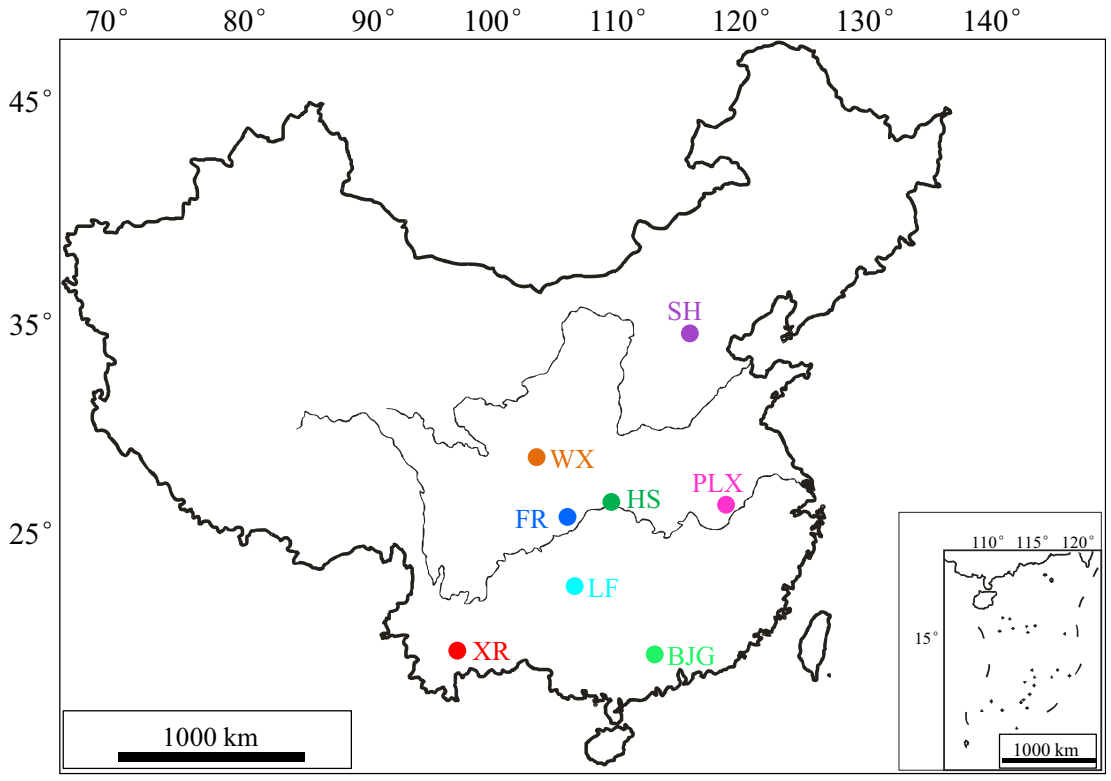

Fig. 1. Map showing the locations of the studied caves.

2. STUDY SITES

All the eight cave sites have already been described in previous studies (Ban et al., 2008; Hu et al., 2008; Luo and Wang, 2008; Zhang et al., 2008, 2012; Cai et al., 2010; Ruan and Hu, 2010; Li et al., 2011, 2012; Duan et al., 2012; Tian et al., 2013) and the basic information of each cave is summarized in Table 1. Among the eight caves, XR, BJG, LF, FR, PLX and HS are under a subtropical monsoon climate, while WX is under a subtropical semi-arid climate and SH is under a temperate monsoon climate. Located within the MRC, each cave area has hot-wet summer and cold-dry winter, with more than 70% of the annual precipitation occurring in the wet season from May to October.

The CO_2 concentration in each cave shows seasonal variation with high values in summer and low values in winter, except HS (Table 1). Unlike other closed caves, HS is well-ventilated and the CO_2 concentration in the cave is relatively stable at about 470 ppmv (Table 1), slightly greater than that of atmospheric concentration.

3. METHODS

In each cave mentioned above, three to five drip sites have been selected for monitoring, a total of thirty-four drips (Table 2, Supplementary Fig. 1). The caves were monitored monthly to bi-monthly, and the measured parameters include surface air temperature and precipitation, cave air temperature, relative humidity, drip rate, and the $\delta^{18}O$ and δD of precipitation and drip waters.

3.1. Field measurements

The surface air temperature outside each cave was recorded automatically by a HOBO Temp/RH Data Logger (H08-003-02), which was fixed in an instrument shelter near to the cave. Precipitation in each cave area was measured automatically by a tipping-bucket rain gauge (Data Logging Rain Gauge-RG3-M; resolution: 0.2 mm). Cave air relative humidity was measured using a handheld HANNA instrument HI 8564 thermo–hygrometer (resolution: RH: 0.1%, accuracy: 2%). The monthly actual evapotranspiration (AET) was calculated from local surface climate data using a water-balance model (Thornthwaite, 1948) as implemented in the USGS Thornthwaite model (McCabe and Markstrom, 2007). For months with missing data, AET were not calculated.

Drip rates were estimated by taking repeat counts of drops over 1 min, reported as drip/minute. For the MP1 and MP2, with continuous dripping, the recharge volume per minute (ml/minute) was measured instead of drip rate (Genty et al., 2001, 2014; Tooth and Fairchild, 2003). This method is only fit for discussing the seasonal variation of discharge, as any drip rate variations occurring more frequently than this sampling period were not monitored.

Table 1
Summary of basic characteristics of the studied caves. "ND" denotes no data. The annual precipitation and mean surface air temperature were calculated based on local meteorological data (AD 1981-2010), with 1σ stand deviation (http://data.cma.cn).

Cave	Latitude, longitude, altitude (m)	Annual precipitation (mm/year)	Annual mean surface air temperature (°C)	Bedrock	Thickness of bedrock (m)	Thickness of soil (cm)	Vegetation	Climate	CO_2 concentration (ppmv)	References
XR	24°07′N,104° 08′E, 1443	1143.3 ± 163.2	16.7 ± 0.5	Massive dolostone Middle Triassic-lower	40–140	0–40	Liana and shrubs	Subtropical monsoon climate	570–12000	Duan et al., 2012
BJG	24°07′N, 113° 21′E, 610	1835.9 ± 405.4	21.2 ± 0.5	Limestone Middle Devonian	>170	ND	Evergreen broad-leaf forest		201–3450	Tian et al., 2013; Tong et al., 2013
LF	26°16′N, 108° 03′E, 600	1211.9 ± 178.4	18.5 ± 0.4	Biogenic limestone Middle to Late Carboniferous	80–140	0–135	Evergreen defoliate broad-leaved forest		482–1842	Luo and Wang, 2008;
FR	29°13′N, 107° 54′E, 480	1026.6 ± 201.5	17.4 ± 0.4	Dolomite Cambrian and Ordovician	300–500	30–90	Evergreen arbor, liana and shrubs		500–2000	Li et al., 2011, 2012
PLX	30°14′N, 117° 32′E, 170	1780.7 ± 356.1	16.1 ± 0.4	Limestone Ordovician	10–50	0–50	Evergreen broad-leaved forest and defoliate broad-leaved forest		500–7000	Zhang et al., 2012
HS	30°27′N, 110° 25′E, 294	1343 ± 297.7	16.5 ± 0.5	Dolomite Cambrian	300	40	Woody perennial plant and shrub-grass		470	Hu et al., 2008; Ruan and Hu, 2010
WX	33°19′N, 105° 00′E, 1200	460.7 ± 94.6	14.9 ± 0.6	Limestone Silurian	30–250	20–100	Grass, arbor and perennial shrubs	Subtropical semi-arid climate	392–1552	Zhang et al., 2008
SH	39°47′N, 115° 56′E, 251	539.2 ± 134.2	12.2 ± 0.6	Limestone, some dolomite Middle Ordovician	30–130	0–100	Shrub and grass, arbor	Temperate monsoon climate	283–2024	Ban et al., 2008; Cai et al., 2010

Table 2
Summary of $\delta^{18}O_p$, $\delta^{18}O_d$, drip rate, cave air temperature and relative humidity for the studied caves. Note that the "Mean" $\delta^{18}O$ of rainwater is the weighted mean $\delta^{18}O_p$ of precipitation. The "$Mean_{in}$" $\delta^{18}O$ of rainwater is the weighted mean $\delta^{18}O_p$ of precipitation when the monthly water balance is greater than zero. The mean drip rate, cave air temperature and relative humidity are shown with 1σ stand deviation. Note that the drip rates of MP1 and MP2 are presented as the recharge volume per minute (ml/minute). The number after each drip site denotes the drip type described in Table 4. *N* is the number of samples.

Cave	Rainfall and drip site	$\delta^{18}O$ (VSMOW, ‰)			Drip rate (drip/minute)	Cave air temperature (°C)	Relative humidity (%)	*N*
		Δ	Mean/$Mean_{in}$	C.V (%)	Mean	Mean	Mean	
XR	Rainwater	12.7	−10.0/−10.7	48.0	/	/	/	18
	X6 (1)	0.6	−9.5	1.8	7.3 ± 9.2	18.7 ± 0.0	100.0 ± 0.0	19
	X7 (1)	0.5	−9.6	1.6	5.6 ± 10.2			18
	X8 (1)	0.8	−9.4	1.7	31.1 ± 53.0			20
	X11 (1)	0.8	−9.3	2.7	1.9 ± 2.0			17
	X13 (1)	0.8	−9.3	2.2	1.5 ± 1.3			20
BJG	Rainwater	10.5	−6.9/−6.9	44.0	/	/	/	26
	BJG2 (1)	0.8	−5.8	3.7	11.8 ± 4.7	21.9 ± 0.5	98.2 ± 3.2	26
	BJG3 (1)	1.2	−5.8	5.5	5.4 ± 8.8	21.8 ± 0.6		26
	BJG6 (2)	3.3	−5.1	21.2	11.6 ± 25.8	19.6 ± 2.1	90.4 ± 6.1	25
	BJG7 (3)	2.9	−5.4	13.5	108.2 ± 178.0	20.4 ± 1.0	94.6 ± 4.9	25
	BJG8 (1)	1.2	−5.9	5.5	31.2 ± 63.2	21.7 ± 0.6	97.4 ± 3.7	23
LF	Rainwater	12.5	−7.2/−6.9	60.0	/	/	/	36
	LF1 (1)	0.8	−7.5	2.6	4.2 ± 1.5	13.9 ± 2.1	94.2 ± 11.3	33
	LF5 (1)	1.4	−6.9	5.6	4.1 ± 4.8			34
	LF6 (3)	5.9	−6.1	27.4	1.0 ± 0.2			37
FR	Rainwater	12.9	−6.3/−6.2	64.0	/	/	/	34
	MP1 (1)	0.8	−7.2	3.0	12.6 ± 7.8	16.4 ± 0.5	97.7 ± 78.5	34
	MP2 (1)	0.9	−7.2	3.0	20.2 ± 6.5	16.6 ± 0.5	84.7 ± 16.1	37
	MP3 (1)	0.9	−7.2	2.8	31.2 ± 6.4	16.3 ± 1.7	84.0 ± 16.1	37
	MP4 (1)	0.5	−7.6	2.1	16.8 ± 3.3	17.6 ± 0.5	86.4 ± 14.8	36
	MP5 (1)	0.5	−7.6	2.1	11.1 ± 3.4			36
PLX	Rainwater	12.4	−7.9/−7.9	42.0	/	/	/	31
	PLX1 (2)	2.5	−7.5	7.6	14.2 ± 6.6	16.3 ± 1.8	97.4 ± 2.6	34
	PLX2 (1)	1.5	−7.3	5.6	0.8 ± 0.2	18.0 ± 0.4	98.0 ± 2.0	31
	PLX3 (2)	2.2	−7.2	7.3	10.4 ± 10.7	17.8 ± 0.3	98.5 ± 1.7	32
	PLX4 (1)	1.0	−7.3	4.5	2.4 ± 1.1	17.9 ± 0.6	98.6 ± 2.1	26
HS	Rainwater	16.8	−7.9/−8.2	67.0	/	/	/	34
	HS4 (1)	1.5	−7.2	4.8	13.0 ± 3.9	18.8 ± 1.8	100.0 ± 0.0	34
	HS6 (1)	1.5	−7.3	4.3	8.0 ± 1.3			34
	HS7 (1)	1.7	−7.4	5.7	4.0 ± 1.0			35
	HS9 (2)	3.1	−6.9	13.8	18.0 ± 22.2			36
WX	Rainwater	10.0	−8.3/	40.0	/	/	/	28
	WX1 (1)	0.6	−9.1	2.4	9.1 ± 3.4	11.8 ± 0.6	96.9 ± 4.9	30
	WX2 (1)	0.9	−9.1	1.9	160.3 ± 109.3	11.2 ± 0.1	100.0 ± 0.3	32
	WX3 (1)	0.6	−9.1	1.8	131.7 ± 22.9			30
SH	Rainwater	10.0	−8.7/−9.4	36.0	/	/	/	24
	PL1 (1)	0.7	−8.9	2.0	5.6 ± 2.4	15.8 ± 1.1	92.0 ± 8.3	28
	PL2 (1)	1.5	−8.8	3.8	0.6 ± 0.2			27
	PL3 (1)	1.0	−8.8	2.3	5.5 ± 5.1			27
	SH (1)	2.3	−8.9	5.2	12.1 ± 7.6	15.5 ± 0.8	92.8 ± 6.0	28
	JG (1)	2.0	−8.9	4.3	47.0 + 46.5	15.4 ± 1.3	89.2 ± 10.1	29

3.2. Water sample collection

Monthly to bi-monthly cumulative precipitation samples were collected above each cave in an open area near the cave entrance. Following the International Atomic Energy Agency (IAEA) protocol, rainwater was collected in a 5 L HDPE bottle with a funnel. A ping-pong ball was placed at the funnel mouth and the bottom of the HDPE bottle was coated with approximately 0.5 cm-thick mineral oil to prevent evaporation. The sub-samples of the homogenized precipitation were removed into pre-cleaned 8 ml glass sealed bottles with no head space for $\delta^{18}O$ and δD analysis.

Cave drip water samples were collected on the same dates as precipitation. The drip water was collected in a 500-ml HDPE bottle that was fixed under the drip site for one night to collect enough water. To investigate whether the "instantaneous" samples are representative of the seepage water isotopic composition between each sampling, we also sampled the coeval accumulated drip water at site X13 for comparison. We did not find significant differences between them (Supplementary Fig. 2). Aliquots for $\delta^{18}O$ and δD analyses were stored in pre-cleaned 8-ml glass sealed bottles with no head space. To minimize evaporation prior to analysis, all rain and drip-water samples were refrigerated.

3.3. Sample analysis

The $\delta^{18}O$ and δD analyses of precipitation and cave drip water collected before 2013 were performed on a cavity ringdown laser spectroscopy (CRDS) (Picarro L2130i Laser Absorption Water Isotopic Spectrometer) in the Key Laboratory of Tibetan Environment Change and Land Surface Processes, Chinese Academy of Sciences. The oxygen isotope measurement of rainwater and drip water samples collected after 2013 were performed on a cavity ringdown laser spectroscopy (CRDS) (Picarro L1102i Laser Absorption Water Isotopic Spectrometer) in the Water Isotopics and Water Rock Interaction Laboratory, Institute of Geology and Geophysics, Chinese Academy of Sciences. The precision was 0.1‰ for $\delta^{18}O$ and 0.5‰ for δD. Results are reported as relative to the standard VSMOW (Vienna Standard Mean Ocean Water). The mean $\delta^{18}O_p$ has been weighted by the corresponding precipitation. For months with missing data, $\delta^{18}O_p$ data were not included in the calculations.

4. RESULTS

4.1. Stable isotopic composition of local precipitation

Raw $\delta^{18}O_p$ data are presented in Supplementary Table 1 and summarized in Tables 2 and 3. At each study site, $\delta^{18}O_p$ demonstrates a seasonal trend with most negative values in the wet season (May to October) and less negative values in the dry season (November to April) (Fig. 2, Table 3), which is in agreement with the large regional and long term study results performed by the Global Network of Isotopes in Precipitation (GNIP) (Johnson and Ingram, 2004; Dayem et al., 2010) and the Chinese Network of Isotopes in Precipitation (CHNIP), with the exception of SH (J. Liu et al., 2014).

Deuterium excess (d) of precipitation ($d = \delta D - 8 \times \delta^{18}O$) (Dansgaard, 1964) exhibits significant seasonal variations with lower values (less than 11.5‰) in the wet season and higher values (greater than 13.0‰) in the dry season (Fig. 2, Table 3). For each cave, although the monthly $\delta^{18}O_p$ value displays a negative correlation with monthly precipitation (MP), only XR, LF and HS are significant at the 95% level (Table 3). For all the caves except SH, there is a negative linear relationship between monthly $\delta^{18}O_p$ and local monthly average surface air temperature (MAT), and for LF, FR and HS, this is significant at the 99% level (Table 3). The correlations between monthly $\delta^{18}O_p$ and MAT and MP are consistent with the results of GNIP (Johnson and Ingram, 2004; Dayem et al., 2010) and CHNIP (J. Liu et al., 2014), long-term investigations, with the exception of SH. The equation of the Local Meteoric Water Line (LMWL) for each cave was established from the $\delta^{18}O$ and δD values of monthly rainwater samples collected during the monitoring period, and compared to the Global Meteoric Water Line defined as $\delta D = 8 \times \delta^{18}O + 10$ (Craig, 1961) (Fig. 3, Table 3). Only at SH, the slope of LMWL is lower than the global average slope of 8 (Fig. 3h, Table 3), which indicates the

Table 3
Summary of seasonal variations of $\delta^{18}O_p$, d, the LMWL and the correlations of $\delta^{18}O_p$-MP and $\delta^{18}O_p$-MAT for the studied caves.

	$\delta^{18}O$ (‰)			d		r		LMWL		
Cave	WS	DS	Δ	WS	DS	$r^{\delta-T}$	$r^{\delta-P}$	Slope	Intercept	n
XR	−10.7	−4.8	5.9	10.7	16.0	−0.41	**−0.63	8.8	19.3	18
BJG	−7.9	−5.2	2.7	9.6	13.1	−0.33	−0.31	8.6	15.2	26
LF	−8.8	−3.6	5.2	9.6	15.7	**−0.68	*−0.38	9.6	20.1	36
FR	−6.8	−3.4	3.4	11.2	19.6	**−0.69	−0.30	9.3	23.2	34
PLX	−7.8	−4.5	3.3	9.8	14.5	−0.31	−0.34	8.7	17.0	31
HS	−9.2	−3.0	6.2	8.7	14.5	**−0.57	*−0.56	8.5	14.2	34
WX	−8.9	−5.2	3.7	10.4	13.7	−0.25	−0.10	8.2	13.1	28
SH	−7.5	−6.4	1.1	8.2	15.9	0.23	−0.17	6.9	3.7	24

"WS" and "DS" denote wet season and dry season, respectively. "$r^{\delta-T}$" and "$r^{\delta-P}$" denote the spearman coefficients of $\delta^{18}O_p$-MAT and $\delta^{18}O_p$-MP, respectively.
** Denotes $P < 0.01$.
* Denotes $P < 0.05$.

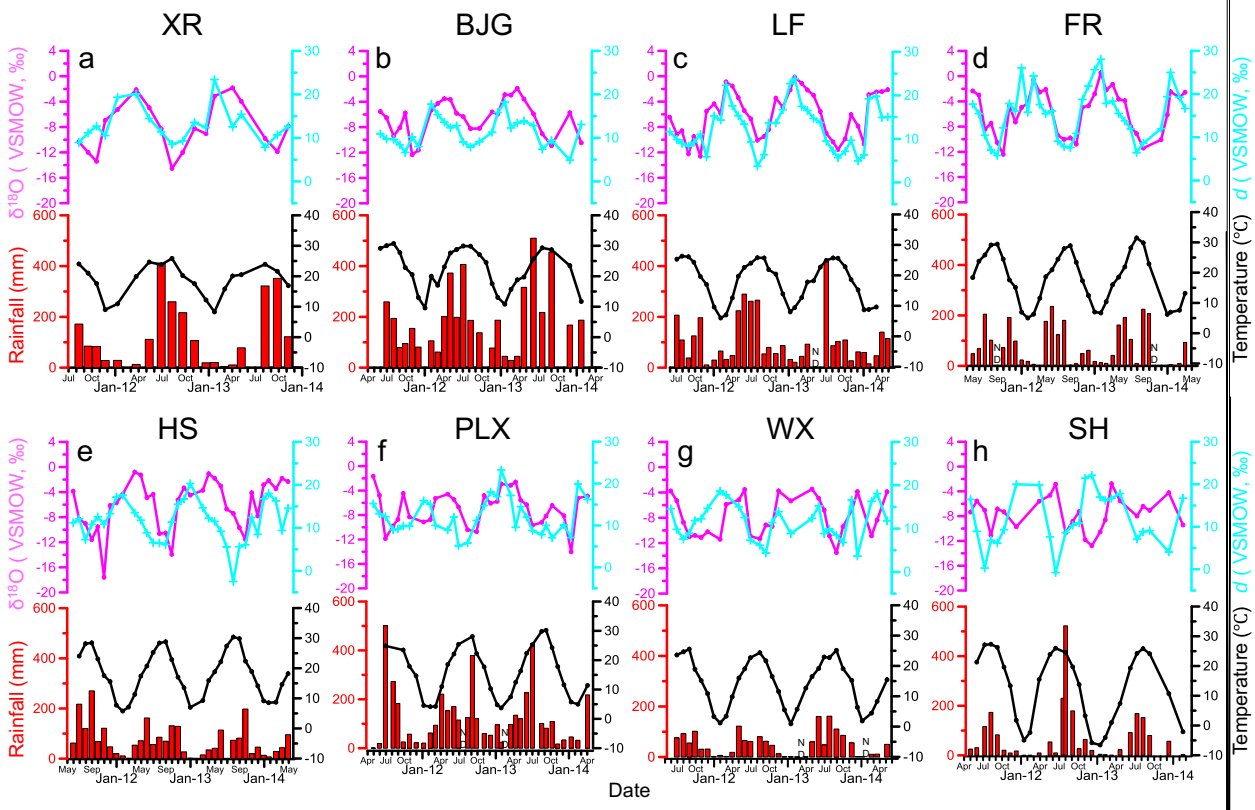

Fig. 2. The time series of $\delta^{18}O_p$, *d*, MP and MAT for the eight caves in this study. "ND" denotes no data.

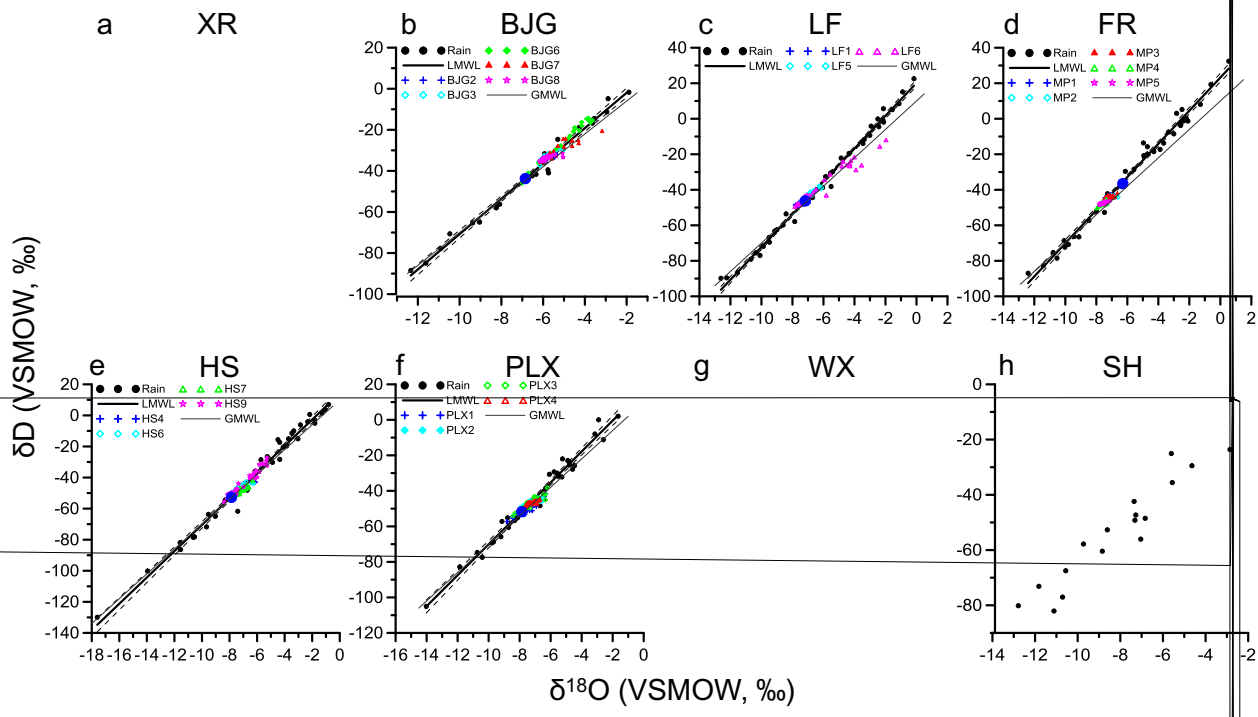

V for abbreviation hereafter). Here, C.V, the quotient of the standard deviation and the mean $\delta^{18}O$ value expressed as a percentage, provides a suitable dimensionless assessment of $\delta^{18}O$ variability; (Type 2) seasonal-variability drips with variable monthly $\delta^{18}O_d$ values, some of which follow the trend of local $\delta^{18}O_p$; (Type 3) medium-variability drips with constant and low $\delta^{18}O_d$ values in the wet season, but with variable and relatively high values in the dry season. All the drip sites in XR, FR, WX and SH are classed as type 1 (Table 2). In the other caves, the drips in an individual cave could be classed into different types: In LF, one drip can be classed as type 3, and the others can be classed as type 1. In HS and PLX, one or two drips can be classed as type 2 and the others can be classed as type 1. In BJG, there are all the three drip types (Table 2).

In general, type 1 are the most widespread drips, which can be found in each cave (Tables 2 and 4). Specially, for sites PL2, SH and JG, although the C.V values are within 6% (Table 2) which are classed as type 1, they still could respond to heavy rain events with ^{18}O-depleted rainwater (Fig. 4h).

5. DISCUSSION

5.1. Controls on the seasonal isotopic variability of precipitation in the MRC

To understand the climatic signals contained in $\delta^{18}O_p$, we need to investigate how atmospheric processes affect it, and which of these has the largest influence. The lack of a significant relationship would indicate that the dominant control on $\delta^{18}O_p$ is another process, or that no single dominant process, or simple set of processes could account for it.

With respect to the seasonal cycle, MAT and $\delta^{18}O_p$ values covary (anti-phased) at all the sites. The highest temperature is in summer and the most negative $\delta^{18}O_p$ value is in summer to early fall. The $\delta^{18}O_p$ values generally then become less negative in winter, when the air temperature is lowest (Fig. 2). Consequently, the monthly $\delta^{18}O_p$ and MAT values are negatively correlated at all sites except SH, which is located at the northern margin of the MRC, although the statistical significance varies (Table 3). The negative $\delta^{18}O_p$-MAT relationship in the MRC is remarkably different from that observed in Europe, which is always positive though the significance and slope vary in site-specific (Celle et al., 2000; Genty et al., 2014).

The underlying positive $\delta^{18}O_p$-MAT relationship observed in high latitude areas (Dansgaard, 1964; Clark and Fritz, 1997) may be masked in the MRC by the correlation between MAT and MP, which are positively correlated at all the eight sites in this study (Fig. 2). To separate out the confounding effects of precipitation that may obscure the underlying $\delta^{18}O_p$-MAT relationship, multiple regressions have been used in previous studies (Johnson and Ingram, 2004; Dayem et al., 2010). Though the partial correlation coefficients tend to be slightly smaller in magnitude than the linear correlation coefficients, they have the same sign, indicating that the strong positive correlations between MAT and MP account for only small portions of the negative correlations between $\delta^{18}O_p$ and MAT (Johnson and Ingram, 2004; Dayem et al., 2010). Therefore, there may be some other independent process that affects both MAT and the $\delta^{18}O_p$ in the MRC and which operates in the opposite direction. Dayem et al. (2010) calculated the relationship between monthly anomalies of $\delta^{18}O_p$ and MAT, and found that they do not generally correlate well with each other. Thus, they argued that the seasonal variation of $\delta^{18}O_p$ and temperature primarily reflect independent processes, both of which are regulated by changes in insolation.

Rainfall amount may also be an important control on the $\delta^{18}O_p$ in the MRC. If this is the case, the negative correlations between MP and monthly $\delta^{18}O_p$ will be expected, as commonly observed in low latitude areas (Dansgaard, 1964; Clark and Fritz, 1997). At all stations in this study, monthly $\delta^{18}O_p$ values are to some extent negatively correlated with MP, but only XR, HS and LF pass the significant test at the 95% level (Table 3). This indicates that although there is a trend of deceasing $\delta^{18}O_p$ values with increasing precipitation, an monthly amount effect (Dansgaard, 1964) can not account for most of the $\delta^{18}O_p$ variations in the MRC, which is in agreement with the results of GNIP (Dayem et al., 2010) and CHNIP (J. Liu et al., 2014), large-regional investigations of $\delta^{18}O_p$ in China.

The amount effect is based on the hypothesis that raindrop evaporation and isotopic equilibrium fractionation tend to increase $\delta^{18}O_p$ in small amounts of rain (Dansgaard, 1964). Therefore, the amount effect will be most apparent where the water source is invariant. However, in the MRC, the water vapor source and the transport paths change greatly due to changes in the atmospheric circulation (Supplementary Fig. 3). In summer, there are three main low latitudinal vapor inflow corridors into China, namely southwestern corridor, south China sea corridor, and southeastern corridor (Supplementary Fig. 3a,b) (Tian et al., 2004; Sun et al., 2006; J. Liu et al., 2008). For most portions of the MRC, the Indian Ocean, through the southwestern corridor, supplies the long-distance water vapor depleted in ^{18}O, but the Pacific Ocean, through southeastern corridor, supplies the short-distance water vapor enriched in ^{18}O (Tan, 2014). Therefore, if the precipitation originates from Pacific Ocean, the short-distance vapor source, the rainwater will be more enriched in ^{18}O than that from Indian Ocean, the long-distance vapor source, whether the former rainfall amount is larger or not than the latter. This scenario may mask the amount effect.

The precipitation patterns and vapor sources also change seasonally in the MRC (Supplementary Fig. 3) (Araguás-Araguás et al., 1998; Yang et al., 2011; Wu et al., 2012). *d* is a characteristic parameter of the source area of the water vapor from which rain originates (Rozanski et al., 1982; Lewis et al., 2013). High humidity during the formation of moist air masses leads to *d* values <10‰, while low humidity at the vapor source typically yields *d* values >10‰ (Clark and Fritz, 1997). *d* of rainwater in each cave area shows the same seasonal variation, with lower values (less than 11.5‰) in the wet season but higher values (greater than 13.0‰) in the dry season

(Fig. 2, Table 3). This suggests that the rainfall in the MRC in the wet season is sourced from tropical air masses, the Pacific Ocean, Indian Ocean or South China Sea (Supplementary Fig. 3a,b), where the humidity is high. In contrast, the rainfall in the dry season is mostly sourced in continental air mass from north, northwest or from local recycled moisture (Supplementary Figs. 3c–f), where the humidity is low, which is in agreement with the previous studies (Araguás-Araguás et al., 1998; Yang et al., 2011; Wu et al., 2012). As noted above, the precipitation in the wet season from tropical maritime air mass has lower $\delta^{18}O_p$ values, while the precipitation in the dry season from continental air mass has higher $\delta^{18}O_p$ values. This could be the reason why monthly $\delta^{18}O_p$ values are to some extent negatively correlated with MP in the MRC.

In short, the variation of $\delta^{18}O_p$ in the MRC is highly complex and a large portion of the variance is unexplained by either temperature or precipitation and may be attributed to some other factors, such as atmospheric circulation (Tan, 2014).

5.2. Relationship between the oxygen isotopic composition of precipitation and drip water

For all caves except XR and SH, the difference between the multi-year weighted mean $\delta^{18}O_p$ of precipitation and the multi-year weighted mean $\delta^{18}O_p$ of precipitation for months when water balance >0 mm is within 0.3‰ (for XR and SH, the difference is 0.7‰) (Table 2). These suggest that the soil moisture deficit is not great enough to affect the infiltration (Fig. 5). In addition, there are some limitations inherent to calculate AET with monthly meteorological data: (1) they will overestimate AET in the MRC, so any water balance deficit will be an overestimate; (2) water balance calculated at monthly time steps can give a negative water balance for the monthly total, but it should be remembered that recharge is still possible from short-duration, high-volume rain events. This scenario has also been observed in Europe (Genty et al., 2014; Comas-Bru and McDermott, 2015).

The monitoring results show that the isotopic composition of most drip waters plots close to or slightly below the corresponding LMWL (Fig. 3). This indicates that most of $\delta^{18}O_d$ reflect that of meteoric water above the caves (Caballero et al., 1996; Cruz, 2005; Pape et al., 2010). The drip waters plotting below the LMWL may have experienced evaporative effects prior to being collected (Pape et al., 2010).

Of the thirty-four drips, twenty-eight drip sites can be classed as type 1 drip (82%) (Table 4), displaying stability in $\delta^{18}O_d$, with C.V less than 6% throughout the study period. This suggests that the residence time of seepage water in these stations is more than three years.

For most of these drips ($n = 17$), the range of $\delta^{18}O_d$ is <1‰ (Table 2). Attenuated seasonal variability of $\delta^{18}O_d$ relative to $\delta^{18}O_p$ has been noted in many previous studies

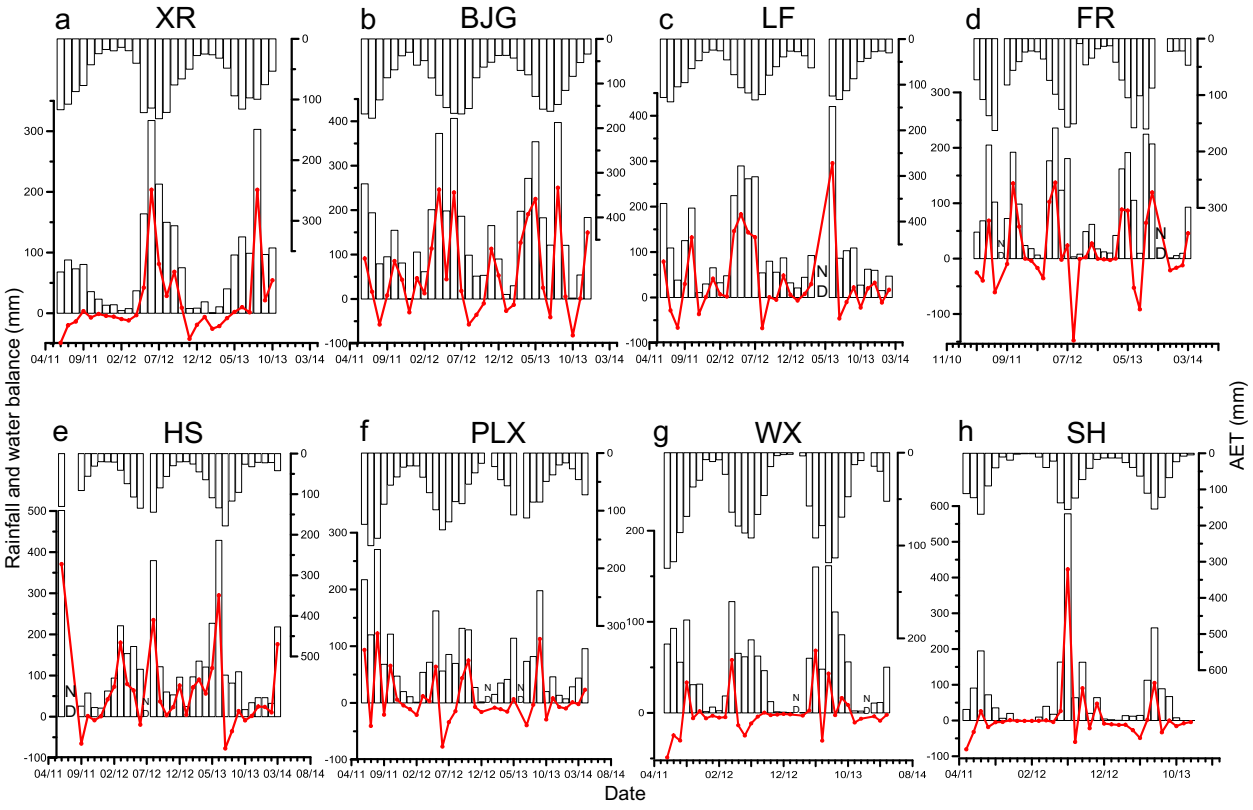

Fig. 5. The time-series of monthly rainfall, calculated actual evapotranspiration (AET) and water balance (red line). (For interpretation of the references to colour in this figure legend, the reader is referred to the web version of this article.)

(Yonge et al., 1985; Caballero et al., 1996; Williams and Fowler, 2002; McDermott, 2004; Genty, 2008; Genty et al., 2014; Luo and Wang, 2008; Onac et al., 2008; Li et al., 2011; Riechelmann et al., 2011). This is always attributed to drip water homogenization via mixing of multi-year precipitation in the soil and epikarst zone above the cave.

Among the twenty-eight of the static drips, for LF1, LF5, PL1, PL2, PL3, SH and JG, the respective mean $\delta^{18}O_d$ value is in agreement with the coeval weighted mean $\delta^{18}O_p$ value (the difference is within 0.3‰) (Table 2). For LF1 and LF5, all the drip water samples plot on the LMWL (Fig. 3c), which reveals their meteoric origin and therefore that almost all of the rainfall events could be infiltrated into the karst unsaturated zone and well mixed. As a consequence, the annual or long-term climatic signals embedded in the isotopic composition of precipitation could be recorded by these drip waters, and in turn, captured by the stalagmites growing under them. However, for PL1, PL2, PL3, SH and JG, all the samples plot below the LWML (Fig. 3h), indicating that they may have experienced some evaporative effects prior to infiltrating into the cave (Fig. 5h). Thus, although the respective average $\delta^{18}O_d$ value is in agreement with the weighted mean value of $\delta^{18}O_p$ (Table 2), this is likely to be the balance of isotopically light infiltration water and subsequent ^{18}O enrichment due to evaporation before reaching to the drip sites (Fig. 5h). Nonetheless, for sites PL2, SH and JG, the $\delta^{18}O_d$ can record the signals of heavy rain events with more ^{18}O-depleted rain water in summer (Fig. 4h). For X6, X7, X8, X11, X13, PLX2, PLX4, HS4, HS6 and HS7, the respective mean $\delta^{18}O_d$ value is slightly higher (within 0.7‰) than the coeval weighted mean $\delta^{18}O_p$ (Table 2). The isotopic enrichment may be attributed to evaporation processes within the soil (Comas-Bru and McDermott, 2015), the epikarst (Cuthbert et al., 2014a) or the loss of some ^{18}O-depleted summer precipitation due to run off or vegetation transpiration (Genty et al., 2014) through which, there is generally no fraction of isotopes (Obrist et al., 2004). Nonetheless, as the $\delta^{18}O_d$ values of these sites are quite constant during the study period, the stalagmites under them may inherit the long-term (maybe more than decadal time scale) climatic signals embedded in the isotopic composition of the water balance (precipitation input and evaporative enrichment or the seasonal recharge) (Baker et al., 2013).

For sites BJG2, BJG3 and BJG8, the mean $\delta^{18}O_d$ value of each site is nearly identical, which is much higher (about 1‰) than the coeval weighted mean $\delta^{18}O_p$ value (Table 2), indicating these drips may be recharged mainly by more strongly evaporated older water stored in the epikarst zone or the large loss of some ^{18}O-depleted summer precipitation due to run off or vegetation transpiration. Even so, as the $\delta^{18}O_d$ value is quite constant during the study period (Fig. 4b), they could probably record the long-term climatic signals (maybe more than decadal time scale) embedded in the local water balance too (Baker et al., 2013).

For sites MP1, MP2, MP3, MP4, MP5, WX1, WX2 and WX3, the respective mean $\delta^{18}O_d$ value is lower (within 1‰) than the coeval weighted mean $\delta^{18}O_p$ value (Table 2). Previous studies attributed this behavior to the selective recharge of seasonal precipitation (White, 1988; Bar-Matthews et al., 1996; Jones et al., 2000; Jones and Banner, 2003; Tooth and Fairchild, 2003; Bradley et al., 2010; Pape et al., 2010; Fairchild and Baker, 2012; Genty et al., 2014.). They argued that there is a precipitation amount threshold, which must be exceeded for water to infiltrating into aquifer, meanwhile, the small rainfall events may be lost by evapotranspiration before infiltrating into the soil or epikarst zones. For FR and WX, during the rainy season, the precipitation is mainly composed of heavy rain events with ^{18}O-depleted rainwater, whereas during the dry season, it is mainly composed of light rain events with ^{18}O-enriched rainwater (Fig. 2d and g). These suggest that parts of ^{18}O-enriched rain in the dry season are too light to exceed the threshold and infiltrate into the epikarst zone. As the $\delta^{18}O_d$ values of each drip site are quite constant during the study period, this kind of drips may be recharged by the well-mixed stored water, which primarily preserves the homogenization of isotopic compositions of the heavy rains in the wet season. Consequently, $\delta^{18}O_s$ recharged by these drips should primarily record the wet season climate conditions as well as some portions of the signals of the dry season in greater timescale.

In general, for type 1 drips, although the $\delta^{18}O_d$ is quite constant, with C.V less than 6% throughout the study period, their drip rates are not necessary static (Fig. 6). Independence between the drip rate and $\delta^{18}O_d$ has already been observed in a previous study (Genty et al., 2014), which was attributed to the existence of a mixing reservoir with a piston flow functioning above these drips. Additionally, for the stalagmite originating from type 1 drips, any seasonal variations of $\delta^{18}O_s$ must reflect in-cave processes (such as the variability of cave temperature) rather than the original sub-annual oxygen isotopic variability in local precipitation (Ruan and Hu, 2010; Feng et al., 2014).

Among the thirty-four drip sites in the eight caves, only four sites (BJG6, HS9, PLX1 and PLX3) (12%) can be classified as type 2 drip (Tables 2 and 4). For sites BJG6 and HS9, although the range of $\delta^{18}O_d$ is narrower than that of rainfall, it tracks the seasonal trend of local $\delta^{18}O_p$ very well, with highest values in the dry season and lowest values in the wet season (Fig 4b, e). Accordingly, $\delta^{18}O_d$ and $\delta^{18}O_p$ show significant positive correlations (the spearman coefficient: $r = 0.67$, $p < 0.01$ for BJG6; $r = 0.65$, $p < 0.01$ for HS9). As the $\delta^{18}O_d$ show seasonal variations, the average $\delta^{18}O_d$ have been weighted by the drip rate of each sties. For HS9, the average $\delta^{18}O_d$ value is in agreement with the coeval local weighted mean $\delta^{18}O_p$ value (Table 2). This suggests that most of the recent precipitation, mixed with some old stored water, can be transmitted through the karst aquifer to this drip within one month, which can also be confirmed by the rapid response of drip rate to precipitation amount (Fig. 6e). This type of drip has been observed in some previous studies (Li et al., 2000; Cruz, 2005; Van Beynen and Febbroriello, 2006; Cobb et al., 2007; Fuller et al., 2008). For BJG6, however, the average $\delta^{18}O_d$ value is higher than the weighted average of coeval $\delta^{18}O_p$ (Table 2). The difference may reflect mixing of freshly infiltrated water with stored water in the epikarst zone which has undergone evaporative enrichment (Tian et al., 2013;

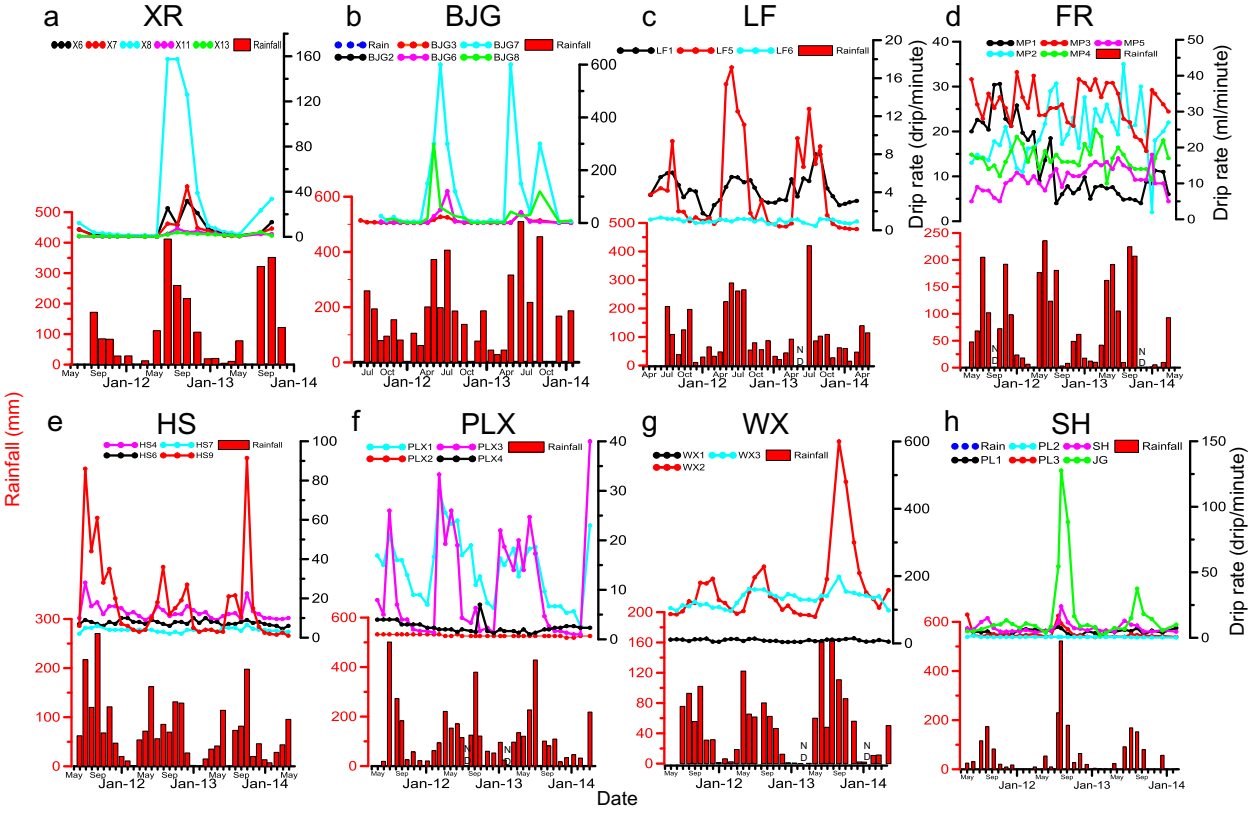

Fig. 6. The time-series of drip rate and MP. "ND" denotes no data. Note that the drip rates of MP1 and MP2 are presented as the recharge volume per minute (ml/minute).

Cuthbert et al., 2014a) or it could also result from the loss of some ^{18}O-depleted summer precipitation due to run off or vegetation transpiration (Genty et al., 2014), while still inheriting most of the seasonal signals of recent $\delta^{18}O_p$. However, for PLX1 and PLX3, although the $\delta^{18}O_d$ values vary seasonally, they do not follow the trend of coeval $\delta^{18}O_p$ well (Fig. 4f) and the average $\delta^{18}O_d$ values are higher than the coeval weighted average of $\delta^{18}O_p$ (Table 2). These indicate that this type of drips can neither inherit the seasonal signal nor the longer-time scale signal of $\delta^{18}O_p$, though their drip rates can response rainfall amount quickly (Fig. 6f). The independence between the drip rate and $\delta^{18}O_d$, suggesting these drips may be recharged through complicated infiltration system, mixing fracture, conduit and piston flow.

In general, for type 2 sites, although all the drip rates can synchronously respond to precipitation amount (Fig. 6), the $\delta^{18}O_d$ does not necessary show a quick response to $\delta^{18}O_p$, depending on the specific drip (Fig. 4).

Among the thirty-four drips, only BJG7 and LF6 can be classed as type 3 drip (6%) (Tables 2 and 4), where the $\delta^{18}O_d$ values are constant and low in the wet season, but variable and relatively high in the dry season (Fig. 4b, c). For BJG7, during the wet season, the mean value of $\delta^{18}O_d$ is −5.7‰, nearly identical to the respective mean value of BJG2, BJG3 and BJG8 in the same cave (Fig. 4b, Table 2). This indicates that, during the wet season, like BJG2, BJG3 and BJG8, the recharge source of BJG7 is mainly the older water stored in the reservoir, mixing with the present-day precipitation. Whereas, during the dry season, though the range of $\delta^{18}O_d$ is lower than that of rainfall, it tracks the pattern of $\delta^{18}O_p$ well, with the average of −5.1‰, which is nearly identical to the weighted average coeval $\delta^{18}O_p$ (−5.2‰). This suggests that, during the dry season, the $\delta^{18}O_d$ can respond to the $\delta^{18}O_p$ timely. Further-

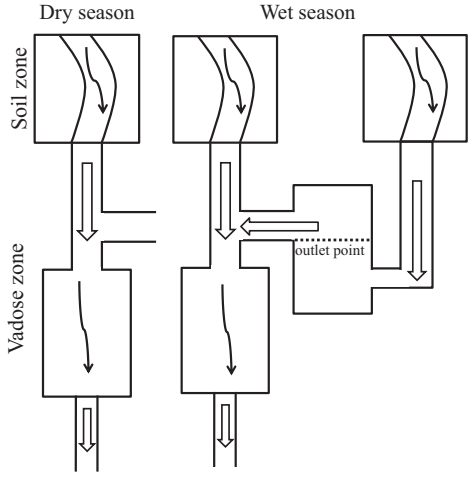

Fig. 7. The model of recharge for drip site BJG7, adapted from Tooth and Fairchild (2003).

more, the drip rate of BJG7 closely resembles the pattern of monthly precipitation (Fig. 6b), indicating that recharge response is consistently rapid during most of the rainfall events. Accordingly, the recharge mode of BJG7 can be inferred as follows. Firstly, there should be well-connected soil and epikarst zone to make the drip rate respond quickly to the monthly precipitation. Secondly, there should be a 'overflow' storage reservoir, with stable older water stored in it. Only when the water storage volume exceeds a certain threshold can the water in the reservoir infiltrate into the cave. For simplicity, the hypothetical karst water flow pathway of BJG7 is illustrated schematically in Fig. 7. During the wet season, the heavy rain can quickly fill the "overflow" storage reservoir, and then the water stored in it, mixed with the new rainwater, can infiltrate into the lower reservoir. Meanwhile, heavy rain could infiltrate directly into the lower reservoir through fractures. Consequently, the drip rates could rise quickly as precipitation amounts increase (Fig. 6b), but the $\delta^{18}O_d$ stays constant, with the value similar to the long-term isotope composition of precipitation stored in the overflow reservoir (Fig. 4b). Whereas, during the dry season, the rainfall is too low for the stored volume to exceed the outlet point of the 'overflow' reservoir, but the rain can still recharge the drips through the fracture connection to the lower reservoir. That explains the observation of $\delta^{18}O_d$ following the pattern of $\delta^{18}O_p$ in the dry season when the drip rate is slow. The recharge mode is similar to the "intermittent response site" as observed by Tooth and Fairchild (2003).

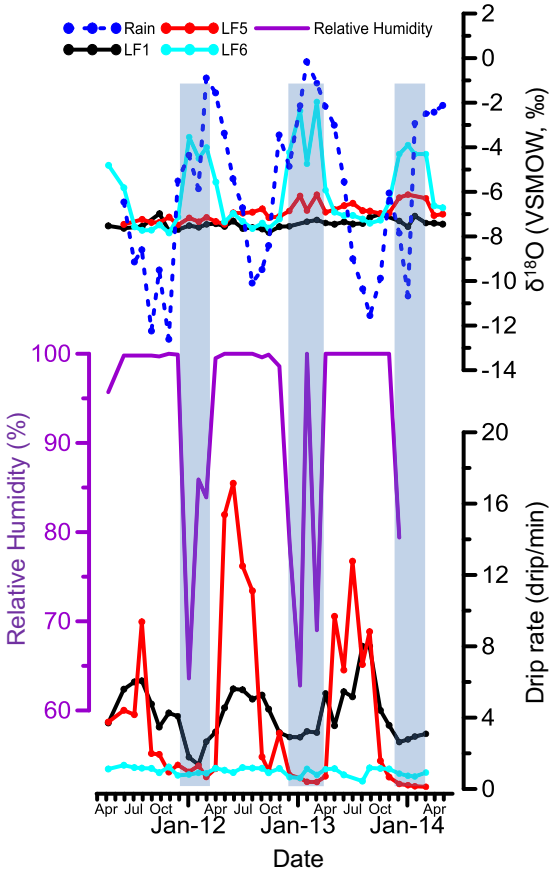

Fig. 8. Comparison between $\delta^{18}O_p$, $\delta^{18}O_d$, cave air relative humidity (RH) and drip rate of drip sites in LF. The blue bars denote the periods when the RH is low and $\delta^{18}O_d$ of LF6 is high. (For interpretation of the references to colour in this figure legend, the reader is referred to the web version of this article.)

For LF6, the pattern of $\delta^{18}O_d$ variation seems similar to that of BJG7, with nearly constant and low values in the wet season but variable and high values in the dry season (Fig. 4c). However, their essential recharge modes may be different. For LF6, during the wet season, the mean $\delta^{18}O_d$ value is −7.3‰, nearly identical to the mean value of LF1 (−7.5‰) (Table 2) in the same cave and the coeval weighted mean $\delta^{18}O_p$ value (−7.2‰) (Fig. 4c). This indicates that, during the wet season, LF6 is recharged mainly by the well-mixed stored water. Whereas, during the dry season, the mean value of $\delta^{18}O_d$ is −4.9‰, about 1.3‰ lighter than the weighted mean value of coeval rainwater (−3.6‰), but 2.3‰ higher than the weighted mean value of local rainwater (−7.2‰). This suggests that, during the dry season, LF6 is not mainly recharged by the coeval precipitation. Furthermore, the drip rate of LF6 is nearly constant at a very low value (average: 0.9 drip/minute) during the study period (Table 2), and there is no significant hydrological response to precipitation (Figs. 6c and 8). The $\delta^{18}O_d$ value may be increased by evaporation inside the cave with low relatively humidity or air circulation (Ingraham et al., 1990; Caballero et al., 1996; Carrasco et al., 2006; Oster et al., 2012; Cuthbert et al., 2014b). In LF, the relative humidity shows seasonal variation, with high values (about 100%) during the wet season, but low values (less than 86%) during the dry season (Fig. 8). However, the other two sites, LF1 and LF5, not far from LF6 (Supplementary Fig. 1c), do not show heavier $\delta^{18}O_d$ values in the dry season (Fig. 4c). The drip rate of LF1 is constant and much greater than that of LF6. While, for LF5, the drip rate shows seasonal variability, with high values in the wet season (greater than LF1) but low values in the dry season (similar or lower than LF6) (Figs. 6c and 8). Meanwhile, LF6 has a higher drip height of 4.5 m than that of LF5 (0.8 m) (Zeng et al., 2015), which may make the drip water undergo longer time during dripping process from stalactite to collector. Therefore, for LF1 and LF5 the drip water could quickly drip into the collector for all or part of the year and experience less evaporation compared to LF6.

In general, since there are complicated recharge systems, the isotopic composition of the stalagmite under this kind of drip cannot be easily used as a climatic proxy.

6. CONCLUSIONS

Based on an approximately three-year (May-2011 to April-2014) monitoring data of eight caves in the MRC, the following conclusions can be drawn:

The monthly $\delta^{18}O_p$ values correlate negatively with MAT at all the sites except SH, although the statistical significance varies, and the correlation is opposite to that expected from the temperature effect in Rayleigh fractionation. Additionally, monthly $\delta^{18}O_p$ values are variably negatively correlated with MP at all the cave sites, but only three

sites are statistically significant at 95%. Therefore, neither the temperature effect nor the amount effect could account for all the variance of $\delta^{18}O_p$ in the MRC, and circulation effect may also be an important factor due to the various sources of water vapor.

About 82% of the thirty-four drip sites are static drips, for which, the $\delta^{18}O_d$ show a remarkable stability since the beginning of the monitoring, although the drip rates are not necessary constant. Thus, regardless of the site-specific discharge systems, there is a commonality among them: the drip water is a mixture of precipitation integrated over relatively long periods (more than three years). This result indicates that most of the $\delta^{18}O_s$ profiles mainly record the average of multi-year climatic signals, modulated by the seasonality of recharge and potential effects of evaporation.

About 12% of the thirty-four drip sites are seasonal drips, for which, the $\delta^{18}O_d$ values vary seasonally and some of them follow the trend of coeval $\delta^{18}O_p$. These drips are mainly recharged by the present-day precipitation through fractures, mixing with some stored water. Accordingly, the seasonal climatic signals embedded in the $\delta^{18}O_p$ could be partly transmitted to some of these drips and in turn to the stalagmites growing under them.

About 6% of the thirty-four drip sites are medium-variability drips, with constant and relative low $\delta^{18}O_d$ values in the wet season but variable and relatively high values in the dry season. The seasonal variability may result from flow switching in the karst or evaporation inside the cave.

In summary, to interpret the climatic signals of $\delta^{18}O_s$, the corresponding hydrological conditions of recharge should be considered, especially the residence time of the infiltrated water.

ACKNOWLEDGEMENTS

We are grateful to Dr. Sulan Nan for providing maps of Supplementary Fig. 3. We also thank students and faculties, too numerous to list, who joined us in field trips to the cave and provided assistance with sampling of rainwater and drip water; the administrative committees of the eight caves in this study for allowing us free access to the caves for observations and sampling. Finally, we are grateful to the journal editor, Prof. McDermott, F. and two anonymous reviewers for their insightful reviews and advices that greatly improved the manuscript.

This research was supported by the National Natural Science Foundation of China (Grant No. 41030103) and the CAS Strategic Priority Research Program (Grant No. XDA05080501).

APPENDIX A. SUPPLEMENTARY DATA

Supplementary data associated with this article can be found, in the online version, at http://dx.doi.org/10.1016/j.gca.2016.03.037.

REFERENCES

Araguás-Araguás L., Froehlich K. and Rozanski K. (1998) Stable isotope composition of precipitation over Southeast Asia. *J. Geophys. Res.* **103**, 721–728.

Ayalon A., Bar-Matthews M. and Sass E. (1998) Rainfall-recharge relationships within a karstic terrain in the Eastern Mediterranean semi-arid region, Israel: $\delta^{18}O$ and δD characteristics. *J. Hydrol.* **207**, 18–31.

Baker A., Asrat A., Fairchild I. J., Leng M. J., Wynn P. M., Bryant C., Genty D. and Umer M. (2007) Analysis of the climate signal contained within $\delta^{18}O$ and growth rate parameters in two Ethiopian stalagmites. *Geochim. Cosmochim. Acta* **71**, 2975–2988.

Baker A., Bradley C. and Phipps S. J. (2013) Hydrological modelling of stalagmite $\delta^{18}O$ response to glacial-interglacial transitions. *Geophys. Res. Lett.* **40**, 3207–3212.

Baldini L. M., McDermott F., Baldini J. U. L., Arias P., Cueto M., Fairchild I. J., Hoffmann D. L., Mattey D. P., Müller W., Nita D. C., Ontañón R., Garciá-Moncó C. and Richards D. A. (2015) Regional temperature, atmospheric circulation, and sea-ice variability within the Younger Dryas Event constrained using a speleothem from northern Iberia. *Earth Planet. Sci. Lett.* **419**, 101–110.

Ban F., Pan G., Zhu J., Cai B. and Tan M. (2008) Temporal and spatial variations in the discharge and dissolved organic carbon of drip waters in Beijing Shihua Cave, China. *Hydro. Process.* **22**, 3749–3758.

Bar-Matthews M., Ayalon A., Matthews A., Sass E. and Halicz L. (1996) Carbon and oxygen isotope study of the active water-carbonate system in a karstic Mediterranean cave: implications for paleoclimate research in semiarid regions. *Geochim. Cosmochim. Acta* **60**, 337–347.

Bar-Matthews M., Ayalon A., Gilmour M., Matthews A. and Hawkesworth C. J. (2003) Sea-land oxygen isotopic relationships from planktonic foraminifera and speleothems in the Eastern Mediterranean region and their implication for paleorainfall during interglacial intervals. *Geochim. Cosmochim. Acta* **67**, 3181–3199.

Bradley C., Baker A., Jex C. N. and Leng M. J. (2010) Hydrological uncertainties in the modelling of cave drip-water $\delta^{18}O$ and the implications for stalagmite palaeoclimate reconstructions. *Quat. Sci. Rev.* **29**, 2201–2214.

Caballero E., Jiménez De Cisneros C. and Reyes E. (1996) A stable isotope study of cave seepage waters. *Appl. Geochem.* **11**, 583–587.

Cai B., Zhu J., Ban F. and Tan M. (2010a) Intra-annual variation of the calcite deposition rate of drip water in Shihua Cave, Beijing, China and its implications for palaeoclimatic reconstructions. *Boreas* **40**, 525–535.

Cai Y., Tan L., Cheng H., An Z., Edwards R. L., Kelly M. J., Kong X. and Wang X. (2010b) The variation of summer monsoon precipitation in central China since the last deglaciation. *Earth Planet. Sci. Lett.* **291**, 21–31.

Carrasco F., Andreo B., Liñán C. and Mudry J. (2006) Contribution of stable isotopes to the understanding of the unsaturated zone of a carbonate aquifer (Nerja Cave, southern Spain). *C.R. Geosci.* **338**, 1203–1212.

Celle H., Daniel M., Mudry J. and Blavoux B. (2000) Rainwater tracing using environmental isotopes in the western Mediterranean region. Case of the region of Avignon (Southeast France). *C.R. Acad. Sci. Ser., Ii Fascicule a–Sci. Terre Et Des Planetes* **331**, 647–650.

Cheng H., Edwards R. L., Broecker W. S., Denton G. H., Kong X., Wang Y., Zhang R. and Wang X. (2009) Ice age terminations. *Science* **326**, 248–252.

Clark I. D. and Fritz P. (1997) *Environmental Isotopes in Hydrogeology*. CRC Press, Boca Raton, New York.

Clemens S. C., Prell W. L. and Sun Y. (2010) Orbital-scale timing and mechanisms driving Late Pleistocene Indo-Asian summer

monsoons: reinterpreting cave speleothem $\delta^{18}O$. *Paleoceanography* **25**, PA4207.
Cobb K. M., Adkins J. F., Partin J. W. and Clark B. (2007) Regional-scale climate influences on temporal variations of rainwater and cave dripwater oxygen isotopes in northern Borneo. *Earth Planet. Sci. Lett.* **263**, 207–220.
Comas-Bru L. and McDermott F. (2015) Data-model comparison of soil–water $\delta^{18}O$ at a temperate site in N. Spain with implications for interpreting speleothem $\delta^{18}O$. *J. Hydrol.* **530**, 216–224.
Craig H. (1961) Isotopic variations in meteoric waters. *Science* **133**, 1702–1703.
Cruz F. (2005) Stable isotope study of cave percolation waters in subtropical Brazil: implications for paleoclimate inferences from speleothems. *Chem. Geol.* **220**, 245–262.
Cruz F., Burns S. J., Karmann I., Sharp W. D. and Vuille M. (2006) Reconstruction of regional atmospheric circulation features during the late Pleistocene in subtropical Brazil from oxygen isotope composition of speleothems. *Earth Planet. Sci. Lett.* **248**, 495–507.
Cuthbert M. O., Rau G. C., Andersen M. S., Roshan H., Rutlidge H., Marjo C. E., Markowska M., Jex C. N., Graham P. W., Mariethoz G., Acworth R. I. and Baker A. (2014a) Evaporative cooling of speleothem drip water. *Sci. Rep.* **4**.
Cuthbert M. O., Baker A., Jex C. N., Graham P. W., Treble P., Andersen M. S. and Acworth R. I. (2014b) Drip water isotopes in semi-arid karst: implications for speleothem paleoclimatology. *Earth Planet. Sci. Lett.* **395**, 194–204.
Dansgaard W. (1964) Stable isotopes in precipitation. *Tellus* **16**, 436–468.
Dayem K. E., Molnar P., Battisti D. S. and Roe G. H. (2010) Lessons learned from oxygen isotopes in modern precipitation applied to interpretation of speleothem records of paleoclimate from eastern Asia. *Earth Planet. Sci. Lett.* **295**, 219–230.
Denniston R. F., González L. A., Asmerom Y., Baker R. G., Reagan M. K. and Bettis, III, E. K. (1999) Evidence for increased cool season moisture during the middle Holocene. *Geology* **27**, 815–818.
Dorale J. A., Gonzalez L. A., Reagan M. K., Pickett D. A., Murrell M. T. and Baker R. G. (1992) A high-resolution record of holocene climate change in speleothem calcite from Cold Water Cave, Northeast Iowa. *Science* **258**, 1626–1630.
Duan W., Cai B., Tan M., Liu H. and Zhang Y. (2012) The growth mechanism of the aragonitic stalagmite laminae from Yunnan Xianren Cave, SW China revealed by cave monitoring. *Boreas* **41**, 113–123.
Duan W., Cheng H., Tan M. and Edwards R. L. (2016) Onset and duration of transitions into Greenland Interstadials 15.2 and 14 in northern China constrained by an annually laminated stalagmite. *Sci. Rep.* **6**, 20844.
Fairchild I. and Baker A. (2012) *Speleothem Science*. Wiley-Blackwell.
Fairchild I. J., Smith C. L., Baker A., Fuller L., Spötl C., Mattey D., McDermott F. and E.I.M.F. (2006) Modification and preservation of environmental signals in speleothems. *Earth Sci. Rev.* **75**, 105–153.
Feng W., Casteel R. C., Banner J. L. and Heinze-Fry A. (2014) Oxygen isotope variations in rainfall, drip-water and speleothem calcite from a well-ventilated cave in Texas, USA: assessing a new speleothem temperature proxy. *Geochim. Cosmochim. Acta* **127**, 233–250.
Fleitmann D., Burns S. J., Mudelsee M., Neff U., Kramers J., Mangini A. and Matter A. (2003) Holocene forcing of the Indian Monsoon Recorded in a Stalagmite from Southern Oman. *Science* **300**, 1737–1739.
Fleitmann D., Burns S., Neff U., Mudelsee M., Mangini A. and Matter A. (2004) Palaeoclimatic interpretation of high-resolution oxygen isotope profiles derived from annually laminated speleothems from Southern Oman. *Quaternary Sci. Rev.* **23**, 935–945.
Fuller L., Baker A., Fairchild I. J., Spötl C., Marca-Bell A., Rowe P. and Dennis P. F. (2008) Isotope hydrology of dripwaters in a Scottish cave and implications for stalagmite palaeoclimate research. *Hydrol. Earth Syst. Sci.* **12**, 1065–1074.
Genty D. (2008) Palaeoclimate research in Villars Cave (Dordogne, SW-France). *Int. J. Speleol.* **37**, 173–191.
Genty D., Baker A. and Vokal B. (2001) Intra- and inter-annual growth rate of modern stalagmites. *Chem. Geol.* **176**, 191–212.
Genty D., Blamart D., Ouahdi R., Gilmour M., Baker A., Jouzel J. and Van-Exter S. (2003) Precise dating of Dansgaard-Oeschger climate oscillations in western Europe from stalagmite data. *Nature* **421**, 833–837.
Genty D., Blamart D., Ghaleb B., Plagnes V., Causse C., Bakalowicz M., Zouari K., Chkir N., Hellstrom J., Wainer K. and Bourges F. (2006) Timing and dynamics of the last deglaciation from European and North African $\delta^{13}C$ stalagmite profiles—comparison with Chinese and South Hemisphere stalagmites. *Quat. Sci. Rev.* **25**, 2118–2142.
Genty D., Labuhn I., Hoffmann G., Danis P. A., Mestre O., Bourges F., Wainer K., Massault M., Van Exter S., Régnier E., Orengo P., Falourd S. and Minster B. (2014) Rainfall and cave water isotopic relationships in two South-France sites. *Geochim. Cosmochim. Acta* **131**, 323–343.
Hu C., Henderson G. M., Huang J., Xie S., Sun Y. and Johnson K. R. (2008) Quantification of Holocene Asian monsoon rainfall from spatially separated cave records. *Earth Planet. Sci. Lett.* **266**, 221–232.
Ingraham N. L., Chapman J. B. and Hess J. W. (1990) Stable isotopes in cave pool systems: Carlsbad Cavern, New Mexico, U.S.A. *Chem. Geol.* **86**, 65–74.
Joe Lambert W. and Aharon P. (2010) Oxygen and hydrogen isotopes of rainfall and dripwater at DeSoto Caverns (Alabama, USA): key to understanding past variability of moisture transport from the Gulf of Mexico. *Geochim. Cosmochim. Acta* **74**, 846–861.
Johnson K. R. (2011) Palaeoclimate: long-distance relationship. *Nat. Geosci.* **4**, 426–427.
Johnson K. R. and Ingram B. L. (2004) Spatial and temporal variability in the stable isotope systematics of modern precipitation in China: implications for paleoclimate reconstructions. *Earth Planet. Sci. Lett.* **220**, 365–377.
Johnson K. R., Hu C., Belshaw N. S. and Henderson G. M. (2006) Seasonal trace-element and stable isotope variations in a Chinese speleothem: the potential for high-resolution paleomonsoon reconstruction. *Earth Planet. Sci. Lett.* **244**, 394–407.
Jones I. C. and Banner J. L. (2003) Estimating recharge thresholds in tropical karst island aquifers: Barbados, Puerto Rico and Guam. *J. Hydrol.* **278**, 131–143.
Jones I. C., Banner J. L. and Humphrey J. D. (2000) Estimating recharge in a tropical Karst Aquifer. *Water Resour. Res.* **36**, 1289–1299.
Kolodny Y., Bar-Matthews M., Ayalon A. and McKeegan K. D. (2003) A high spatial resolution $\delta^{18}O$ profile of a speleothem using an ion-microprobe. *Chem. Geol.* **197**, 21–28.
Lachniet M. S. (2009) Climatic and environmental controls on speleothem oxygen-isotope values. *Quat. Sci. Rev.* **28**, 412–432.
Lauritzen S. E. (1995) High-resolution paleotemperature proxy record for the last interglaciation based on Norwegian Speleothems. *Quat. Res.* **43**, 133–146.

Lee J. E., Risi C., Fung I., Worden J., Scheepmaker R. A., Lintner B. and Frankenberg C. (2012) Asian monsoon hydrometeorology from TES and SCIAMACHY water vapor isotope measurements and LMDZ simulations: implications for speleothem climate record interpretation. *J. Geophys. Res.* **117**, D15112.

LeGrande A. N. and Schmidt G. A. (2009) Sources of Holocene variability of oxygen isotopes in paleoclimate archives. *Clim. Past.* **5**, 441–455.

Lewis S. C., LeGrande A. N., Kelley M. and Schmidt G. A. (2013) Modeling insights into deuterium excess as an indicator of water vapor source conditions. *J. Geophys. Res. Atmos.* **118**, 243–262.

Li B., Yuan D., Qin J., Lin Y. and Zhang M. (2000) Oxygen and carbon isotopic characteristics of rainwater, drip water and present speleothems in a cave in Guilin area, and their environmental meanings. *Sci. China Ser. D-Earth Sci.* **43**, 277–285.

Li T., Shen C., Li H., Li J., Chiang H., Song S., Yuan D., Lin C., Gao P., Zhou L., Wang J., Ye M., Tang L. and Xie S. Y. (2011) Oxygen and carbon isotopic systematics of aragonite speleothems and water in Furong Cave, Chongqing, China. *Geochim. Cosmochim. Acta* **75**, 4140–4156.

Li T., Li H., Xiang X., Kuo T. S., Li J., Zhou F., Chen H. and Peng L. (2012) Transportation characteristics of $\delta^{13}C$ in the plants-soil-bedrock-cave system in Chongqing karst area. *Sci. China. Earth Sci.* **55**, 685–694.

Liu D., Wang Y., Cheng H., Edwards R. L., Kong X., Wang X., Wu J. and Chen S. (2008) A detailed comparison of Asian Monsoon intensity and Greenland temperature during the Allerød and Younger Dryas events. *Earth Planet. Sci. Lett.* **272**, 691–697.

Liu J., Song X., Yuan G., Sun X., Liu X., Wang Z. and Wang S. (2008) Stable isotopes of summer monsoonal precipitation in southern China and the moisture sources evidence from $\delta^{18}O$ signature. *J. Geogr. Sci.* **18**, 155–165.

Liu J., Song X., Yuan G. and Sun X. (2014) Stable isotopic compositions of precipitation in China. *Tellus B.* **66**, 22567.

Liu Z., Wen X., Brady E. C., Otto-Bliesner B., Yu G., Lu H., Cheng H., Wang Y., Zheng W., Ding Y., Edwards R. L., Cheng J., Liu W. and Yang H. (2014) Chinese cave records and the East Asia Summer Monsoon. *Quat. Sci. Rev.* **83**, 115–128.

Luo W. and Wang S. (2008) Transmission of oxygen isotope signals of precipitation-soil water-drip water and its implications in Liangfeng Cave of Guizhou, China. *Chin. Sci. Bull.* **53**, 3364–3370.

Luo W., Wang S., Zeng G., Zhu X. and Liu W. (2014) Daily response of drip water isotopes to precipitation in Liangfeng Cave, Guizhou Province, SW China. *Quat. Int.* **349**, 153–158.

Ma Z., Cheng H., Tan M., Edwards R. L., Li H., You C., Duan W., Wang X. and Kelly M. J. (2012) Timing and structure of the Younger Dryas event in northern China. *Quat. Sci. Rev.* **41**, 83–93.

Maher B. A. (2008) Holocene variability of the East Asian summer monsoon from Chinese cave records: a re-assessment. *Holocene* **18**, 861–866.

McCabe G. J. and Markstrom S. L. (2007) *A Monthly Water-balance Model Driven by a Graphical User Interface*, U.S. Geological Survey Open-File report 2007-1088.

McDermott F. (2004) Palaeo-climate reconstruction from stable isotope variations in speleothems: a review. *Quat. Sci. Rev.* **23**, 901–918.

McDermott F., Frisia S., Huang Y., Longinelli A., Spiro B., Heaton T. H. E., Hawkesworth C. J., Borsato A., Keppens E. and Fairchild I. J. (1999) Holocene climate variability in Europe: evidence from $\delta^{18}O$, textural and extension-rate variations in three speleothems. *Quat. Sci. Rev.* **18**, 1021–1038.

McDermott F., Mattey D. P. and Hawkesworth C. (2001) Centennial-scale holocene climate variability revealed by a high-resolution speleothem $\delta^{18}O$ record from SW Ireland. *Science* **294**, 1328–1331.

Moseley G. E., Spötl C., Svensson A., Cheng H., Brandstätter S. and Edwards R. L. (2014) Multi-speleothem record reveals tightly coupled climate between central Europe and Greenland during Marine Isotope Stage 3. *Geology* **42**, 1043–1046.

Neff U., Burns S. J., Mangini A., Mudelsee M., Fleitmann D. and Matter A. (2001) Strong coherence between solar variability and the monsoon in Oman between 9 and 6 kyr ago. *Nature* **411**, 290–293.

Obrist D., Yakir D. and Arnone, III, J. A. (2004) Temporal and spatial patterns of soil water following wildfire-induced changes in plant communities in the Great Basin in Nevada. *USA Plant Soil* **262**, 1–12.

Onac B. P., Constantin S., Lundberg J. and Lauritzen S.-E. (2002) Isotopic climate record in a Holocene stalagmite from Ursilor Cave (Romania). *J. Quat. Sci.* **17**, 319–327.

Onac B. P., Pace-Graczyk K. and Atudirei V. (2008) Stable isotope study of precipitation and cave drip water in Florida (USA): implications for speleothem-based paleoclimate studies. *Isot. Environ. Health Sci.* **44**, 149–161.

Orland I. J., Bar-Matthews M., Kita N. T., Ayalon A., Matthews A. and Valley J. W. (2009) Climate deterioration in the Eastern Mediterranean as revealed by ion microprobe analysis of a speleothem that grew from 2.2 to 0.9 ka in Soreq Cave, Israel. *Quat. Res.* **71**, 27–35.

Orland I. J., Bar-Matthews M., Ayalon A., Matthews A., Kozdon R., Ushikubo T. and Valley J. W. (2012) Seasonal resolution of Eastern Mediterranean climate change since 34 ka from a Soreq Cave speleothem. *Geochim. Cosmochim. Acta* **89**, 240–255.

Orland I. J., Burstyn Y., Bar-Matthews M., Kozdon R., Ayalon A., Matthews A. and Valley J. W. (2014) Seasonal climate signals (1990–2008) in a modern Soreq Cave stalagmite as revealed by high-resolution geochemical analysis. *Chem. Geol.* **363**, 322–333.

Oster J. L., Montañez I. P. and Kelley N. P. (2012) Response of a modern cave system to large seasonal precipitation variability. *Geochim. Cosmochim. Acta* **91**, 92–108.

Pape J. R., Banner J. L., Mack L. E., Musgrove M. and Guilfoyle A. (2010) Controls on oxygen isotope variability in precipitation and cave drip waters, central Texas, USA. *J. Hydrol.* **385**, 203–215.

Pausata F. S., Battisti D. S., Nisancioglu K. H. and Bitz C. M. (2011) Chinese stalagmite $\delta^{18}O$ controlled by changes in the Indian monsoon during a simulated Heinrich event. *Nat. Geosci.* **4**, 474–480.

Riechelmann D. F. C., Schröder-Ritzrau A., Scholz D., Fohlmeister J., Spötl C., Richter D. K. and Mangini A. (2011) Monitoring Bunker Cave (NW Germany): a prerequisite to interpret geochemical proxy data of speleothems from this site. *J. Hydrol.* **409**, 682–695.

Rozanski K., Sonntag C. and Münnich K. O. (1982) Factors controlling stable isotope composition of European precipitation. *Tellus* **34**, 142–150.

Ruan J. and Hu C. (2010) Seasonal variations and environmental controls on stalagmite calcite crystal growth in Heshang Cave, central China. *Chin. Sci. Bull.* **55**, 3929–3935.

Spötl C., Mangini A. and Richards D. A. (2006) Chronology and paleoenvironment of Marine Isotope Stage 3 from two high-elevation speleothems, Austrian Alps. *Quat. Sci. Rev.* **25**, 1127–1136.

Sun J., Wei J. and Zhao S. (2006) The weather and its circulation in summer of 2005. *Clim. Environ. Res.* **11**, 138–154 (in Chinese with English abstract).

Tan M. (2014) Circulation effect: response of precipitation $\delta^{18}O$ to the ENSO cycle in monsoon regions of China. *Clim. Dynam.* **42**, 1067–1077.

Tang K. and Feng X. (2001) The effect of soil hydrology on the oxygen and hydrogen isotopic compositions of plants' source water. *Earth Planet. Sci. Lett.* **185**, 355–367.

Thornthwaite C. W. (1948) An approach toward a rational classification of climate. *Geograph. Rev.* **38**, 55–94.

Tian H., Guo P. and Lu W. (2004) Characteristics of vapor inflow corridors related to summer rainfall in China and impact factors. *J. Trop. Meteorol.* **20**, 401–408 (in Chinese with English abstract).

Tian L., Zhou H. and Duan W. (2013) The evaporation effect on transmission of oxygen isotope signal of drip water in Baojinggong, Guangdong revealed by cave monitoring. *Quat. Sci.* **33**, 618–620 (in Chinese with English abstract).

Tong X., Zhou H., Huang Y. H. B. and Zhou L. (2013) Spatio-temporal variation of air CO_2 concentration in Baojinggong Cave, Guangdong, China. *Trop. Geogr.* **33**, 439–443 (in Chinese with English abstract).

Tooth A. F. and Fairchild I. J. (2003) Soil and karst aquifer hydrological controls on the geochemical evolution of speleothem-forming drip waters, Crag Cave, southwest Ireland. *J. Hydrol.* **273**, 51–68.

Treble P. C., Chappell J., Gagan M. K., McKeegan K. D. and Harrison T. M. (2005) In situ measurement of seasonal $\delta^{18}O$ variations and analysis of isotopic trends in a modern speleothem from southwest Australia. *Earth Planet. Sci. Lett.* **233**, 17–32.

Treble P. C., Schmitt A. K., Edwards R. L., McKeegan K. D., Harrison T. M., Grove M., Cheng H. and Wang Y. J. (2007) High resolution Secondary Ionisation Mass Spectrometry (SIMS) $\delta^{18}O$ analyses of Hulu Cave speleothem at the time of Heinrich Event 1. *Chem. Geol.* **238**, 197–212.

Van Beynen P. and Febbroriello P. (2006) Seasonal isotopic variability of precipitation and cave drip water at Indian Oven Cave, New York. *Hydrol. Process.* **20**, 1793–1803.

Wackerbarth A., Scholz D., Fohlmeister J. and Mangini A. (2010) Modelling the $\delta^{18}O$ value of cave drip water and speleothem calcite. *Earth Planet. Sci. Lett.* **299**, 387–397.

Wang H. and Chen H. (2012) Climate control for southeastern China moisture and precipitation: Indian or East Asian monsoon? *J. Geophys. Res. Atmos.* **117**, D12109.

Wang Y., Cheng H., Edwards R. L., An Z., Wu J., Shen C. and Dorale J. A. (2001) A high-resolution absolute-dated late Pleistocene monsoon record from Hulu Cave, China. *Science* **294**, 2345–2348.

Wang Y., Cheng H., Edwards R. L., He Y., Kong X., An Z., Wu J., Kelly M. J., Dykoski C. A. and Li X. (2005) The Holocene Asian Monsoon: links to solar changes and North Atlantic Climate. *Science* **308**, 854–857.

Wang Y., Cheng H., Edwards R. L., Kong X., Shao X., Chen S., Wu J., Jiang X., Wang X. and An Z. (2008) Millennial- and orbital-scale changes in the East Asian monsoon over the past 224,000 years. *Nature* **451**, 1090–1093.

White B. (1988) *Geomorphology and Hydrology of Karst Terrains*. Oxford University Press, New York, Oxford.

Williams P. P. W. and Fowler A. (2002) Relationship between oxygen isotopes in rainfall, cave percolation waters and speleothem calcite at Waitomo, New Zealand. *J. Hydrol. New. Zeal.* **41**, 53–70.

Wu H., Zhang X., Guan H., Sun G., Huang Y. and Zhang T. (2012) Influences of different moisture sources on δD and $\delta^{18}O$ in Precipitation in Changsha, Hunan Province. *J. Nat. Resour.* **27**, 1404–1414 (in Chinese with English abstract).

Yang X., Yao T., Yang W., Yu W. and Qu D. (2011) Co-existence of temperature and amount effects on precipitation $\delta^{18}O$ in the Asian monsoon region. *Geophys. Res. Lett.* **38**, L21809.

Yonge C., Ford D., Gray J. and Schwarcz H. (1985) Stable isotope studies of cave seepage water. *Chem. Geol.* **58**, 97–105.

Yuan D., Cheng H., Edwards R. L., Dykoski C. A., Kelly M. J., Zhang M., Qing J., Lin Y., Wang Y., Wu J., Dorale J. A., An Z. and Cai Y. (2004) Timing, duration, and transitions of the last interglacial Asian monsoon. *Science* **304**, 575–578.

Zeng G., Luo W., Wang S. and Du X. (2015) Hydrogeochemical and climatic interpretations of isotopic signals from precipitation to drip waters in Liangfeng Cave, Guizhou Province, China. *Environ. Earth Sci.* **74**, 1509–1519.

Zhang P., Cheng H., Edwards R. L., Chen F., Wang Y., Yang X., Liu J., Tan M., Wang X., Liu J., An C., Dai Z., Zhou J., Zhang D., Jia J., Jin L. and Johnson K. R. (2008) A test of climate, sun, and culture relationships from an 1810-Year Chinese cave record. *Science* **322**, 940–942.

Zhang W., Duan W., Wu J. and Tan M. (2012) One of the important causes of lack of active speleothem in Nanjing Hulu cave: salting-in effect? A comparative study with Penglaixian cave, Anhui under the same climate conditions. *Quat. Sci.* **32**, 361–368 (in Chinese with English abstract).

Associate editor: F. McDermott